Significantly Sensitized Ternary Blend Polymer Solar Cells with a Very Small Content of the Narrow-Band Gap Third Component That Utilizes Optical Interference

AUTHOR(S):

Saito, Masahiko; Tamai, Yasunari; Ichikawa, Hiroyuki; Yoshida, Hiroyuki; Yokoyama, Daisuke; Ohkita, Hideo; Osaka, Itaru

CITATION:

Saito, Masahiko ...[et al]. Significantly Sensitized Ternary Blend Polymer Solar Cells with a Very Small Content of the Narrow-Band Gap Third Component That Utilizes Optical Interference. Macromolecules 2020, 53(23): 10623-10635

ISSUE DATE:

2020-12-08

URL:

http://hdl.handle.net/2433/259821

Significantly Sensitized Ternary Blend Polymer Solar Cells with Very Small Content of Narrow-Bandgap Third Component That Utilizes Optical Interference

Masahiko Saito,[1] Yasunari Tamai,[2] Hiroyuki Ichikawa,[3] Hiroyuki Yoshida,[3,4] Daisuke Yokoyama,[5] Hideo Ohkita,[2]* Itaru Osaka[1]**

[1]Department of Applied Chemistry, Graduate School of Engineering, Hiroshima University, 1-4-1 Kagamiyama, Higashi-Hiroshima, Hiroshima 739-8527, Japan

[2]Department of Polymer Chemistry, Graduate School of Engineering, Kyoto University, Katsura, Kyoto 615-8510, Japan.

[3]Graduate School of Engineering, Chiba University, 1-33 Yayoi-cho, Inage-ku, Chiba 263-8522, Japan

[4]Molecular Chirality Research Center, Chiba University, 1-33 Yayoi-cho, Inage-ku, Chiba 263-8522, Japan

[5]Department of Organic Materials Science and Research Center for Organic Electronics (ROEL), Yamagata University, 4-3-16 Jonan, Yonezawa, Yamagata 992-8510, Japan

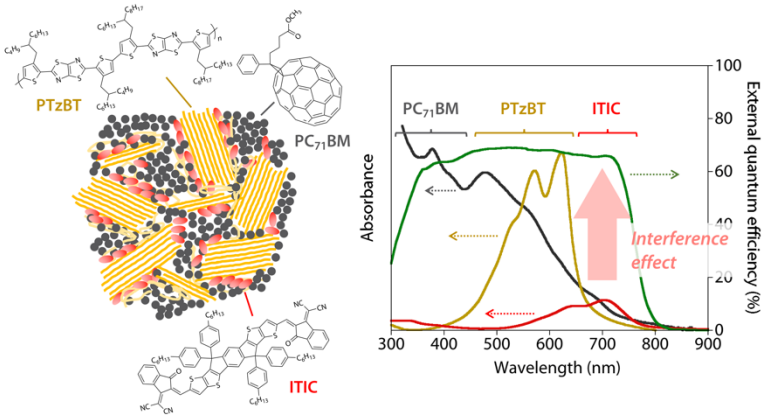

TOC graphic

Abstract

Increasing photon harvest is an essential issue in improving the efficiency of organic photovoltaics. Here, we study ternary blend polymer solar cells that are composed of a thiazolothiazole-based crystalline semiconducting polymer and a fullerene derivative as the host binary system and a very small content of a series of narrow-bandgap non-fullerene acceptors as the third-component sensitizer that is selectively located at the interface between the host donor and acceptor. Surprisingly, the cells give an external quantum efficiency in the sensitizer absorption range that is as high as that in the polymer absorption range despite the fact that the optimal sensitizer content is only 6 wt%, which is far smaller than the host polymer contents. This leads to significantly improved photocurrents and, in turn, high power conversion efficiencies relative to the binary blend cell. Such pronounced sensitization is found to originate in the markedly amplified sensitizer absorption owing to the optical interference effect of the more than 300-nm-thick photoactive layers. In parallel, the ternary blend system realizes markedly reduced photon energy loss, which is also important for the PCE improvement, and high thermal stability. With such excellent features, we believe that the sensitized ternary blend cells have exceptional possibilities and that exploring more well-matched material combinations would improve the performance further.

INTRODUCTION

Organic photovoltaics (OPVs) based on bulk-heterojunction (BHJ) photoactive layers that use semiconducting polymers have been arousing profound interest as flexible, lightweight, and semitransparent solar cells, and can be produced by solution processes that involve low-cost and low-energy methodologies.[1-2] A critical issue in OPVs is the improvement of the power conversion efficiency (PCE). One of the important strategies for PCE improvement is to harvest as many incident photons as possible because this would lead to a large photocurrent. A simple approach to increase photon harvest is to red-shift the absorption range of the semiconducting polymers to match the solar spectrum.[3-5] A large number of semiconducting polymers as both p-type and n-type semiconductors (electron donor and acceptor) with long-wavelength absorption, i.e., a narrow optical bandgap, have been developed in the last decade.[4,6-10] More recently, small-molecule non-fullerene acceptors (NFAs) with long-wavelength absorption have been intensively synthesized and investigated.[11-13]

Photoactive layer thickening can also increase photon harvest owing to the increased volume of the semiconducting materials.[14-23] Whereas the use of a thick photoactive layer potentially increases the photocurrent of the cell, it often causes a severe decrease in the fill factor (FF) and thus the PCE, most likely due to the relatively low charge carrier mobility of the materials. Thus, the optimal photoactive layer thickness is typically limited to around 100 nm in OPVs,[24-25] even for the state-of-the-art BHJ system that uses NFAs.[12] Examples of thick-layered OPV cells have been limited to the BHJ system composed of regioregular poly(3-hexylthiophene) (P3HT) and [6,6]-phenyl-C_{61} (or C_{71})-butyric acid methyl ester ($PC_{61}BM$ or $PC_{71}BM$).[14-16] However, recent studies have shown that the use of some semiconducting polymers with high crystallinity other than P3HT, when combined with PCBMs, also enable a thick photoactive layer.[17-19,21-23] On the other hand, managing the optical interference is another effective way to maximize photon harvest.[17,26-28] The absorption within the photoactive layer does not linearly increase with the thickness and maximizes at some specific thickness because of the optical interference effect originating in the light reflection at the metal electrode. Thus, careful control

of the photoactive layer thickness can boost the absorption. In order to realize this, the use of a semiconducting polymer enabling a thicker photoactive layer is indispensable.

Ternary blend systems, in which three materials with different absorption ranges compose a single photoactive layer, have also been intensively studied as they can likewise effectively harvest incident light over a wide wavelength range that binary blend systems cannot cover. The ternary blends are composed of either two donors and one acceptor or one donor and two acceptors in which each pair of the donor and the acceptor independently undergoes photoinduced charge transfer in general, although several other modes (mechanisms) have been proposed as well.[29-35] Apart from ternary blends with such "parallel-like" systems, "sensitized" systems have also been studied. One of the interesting sensitized systems includes the ternary blends in which the blend of P3HT and $PC_{61}BM$ (or $PC_{71}BM$) is used as the host binary system and a small amount (5–20 wt%) of a long-wavelength absorber (narrow-bandgap) dye, such as diketopyrrolopyrrole,[36-37] phthalocyanine,[38-42] or squaraine[43-44] derivatives, is added as the third component (sensitizer). In these systems, the small-content third component absorbs light and injects the generated charge carriers into the host donor and acceptor. Nguyen and co-workers first demonstrated sensitization in a BHJ polymer solar cell using a diketopyrrolopyrrole molecule.[36] Ohkita and co-workers systematically studied sensitized ternary blend systems using a series of phthalocyanine dyes[38-42] and found that the phthalocyanine dye molecules were selectively located at the interface between P3HT and $PC_{61}BM$, in which the surface energy of each material and the crystallization of the host materials were the driving force for the interfacial distribution.[40-42] This resulted in energy levels in a cascade manner at the interface of these three components, which effectively allowed the charge generation. It is also interesting to note that in such ternary blend systems, an energy transfer from P3HT to the dye sweeps out the excitons buried in the P3HT domains.[40,43] As such, the sensitized ternary blend system is believed to be a promising strategy for PCE improvement in OPVs. However, only P3HT has been used as the host crystalline polymer in that system, and thus the overall PCE has been limited to less than 5%. Although studies

have focused on increasing sensitizer content to increase photon harvest,[42,45] a large sensitizer content has always been detrimental to OPV performance, most likely due to the unfavorable location of the sensitizer and/or the destruction of the blend morphology. Further, theoretical simulation predicted that in such type of sensitized ternary system, PCEs for combinations of narrow-bandgap host donor polymer and wide-bandgap sensitizer would exceed hose for reverse combinations.[46] This is because it is advantageous to allow the donor polymer, which has much larger content than the sensitizer, to absorb the photon-abundant red portion of the solar spectrum.

Here, we studied a ternary blend system in which we employed a wide-bandgap polymer based on thiophene and thiazolothiazole (PTzBT) having high crystallinity and face-on backbone orientation as the host donor polymer,[21,23,47] which was combined with $PC_{71}BM$ as the pair for the host binary system, and a small amount of an NFA, which has a narrower bandgap than PTzBT, as the third-component sensitizer (**Figure 1a**). The NFAs used here are ITIC,[48] IT-4F,[49] IT-M,[50] and IEICO-4F[51] (**Figure 1b**), where the former three have the same molecular frame with a similar absorption range but with different energy levels, and the latter has a red-shifted absorption range relative to the former. The PTzBT-based sensitized ternary blend system in which the optimal NFA content is as small as 6 wt% provides significantly improved PCEs compared to the PTzBT/$PC_{71}BM$ binary system. The highest performance was observed with a photoactive layer of more than 300 nm thickness, which was comparable to the PTzBT:$PC_{71}BM$ binary blend cell. To our surprise, the external quantum efficiency (EQE) in the NFA absorption range was as high as that in the host polymer absorption range despite the fact that the NFA content is only 6 wt%, which is far smaller than the host polymer content. Importantly, we found that the optical interference effect plays an important role in harvesting the red photons. The result indicates that by utilizing the optical interference effect, the addition of a very small amount of narrow-bandgap sensitizer would be sufficient to harvest additional photons and lead to a high PCE if a thick photoactive layer is used. Such materials combination is contrary to the desirable combination in theory as mentioned above.[46] Further, this system can generate higher open-

circuit voltage (V_{OC}) than the host binary system, leading to significantly reduced photon energy loss (E_{loss}). In addition, the ternary blend cell shows markedly improved thermal stability compared to the binary blend cell. We believe that these results would considerably expand the possibilities of sensitized ternary blend cells in improving the performance of OPVs.

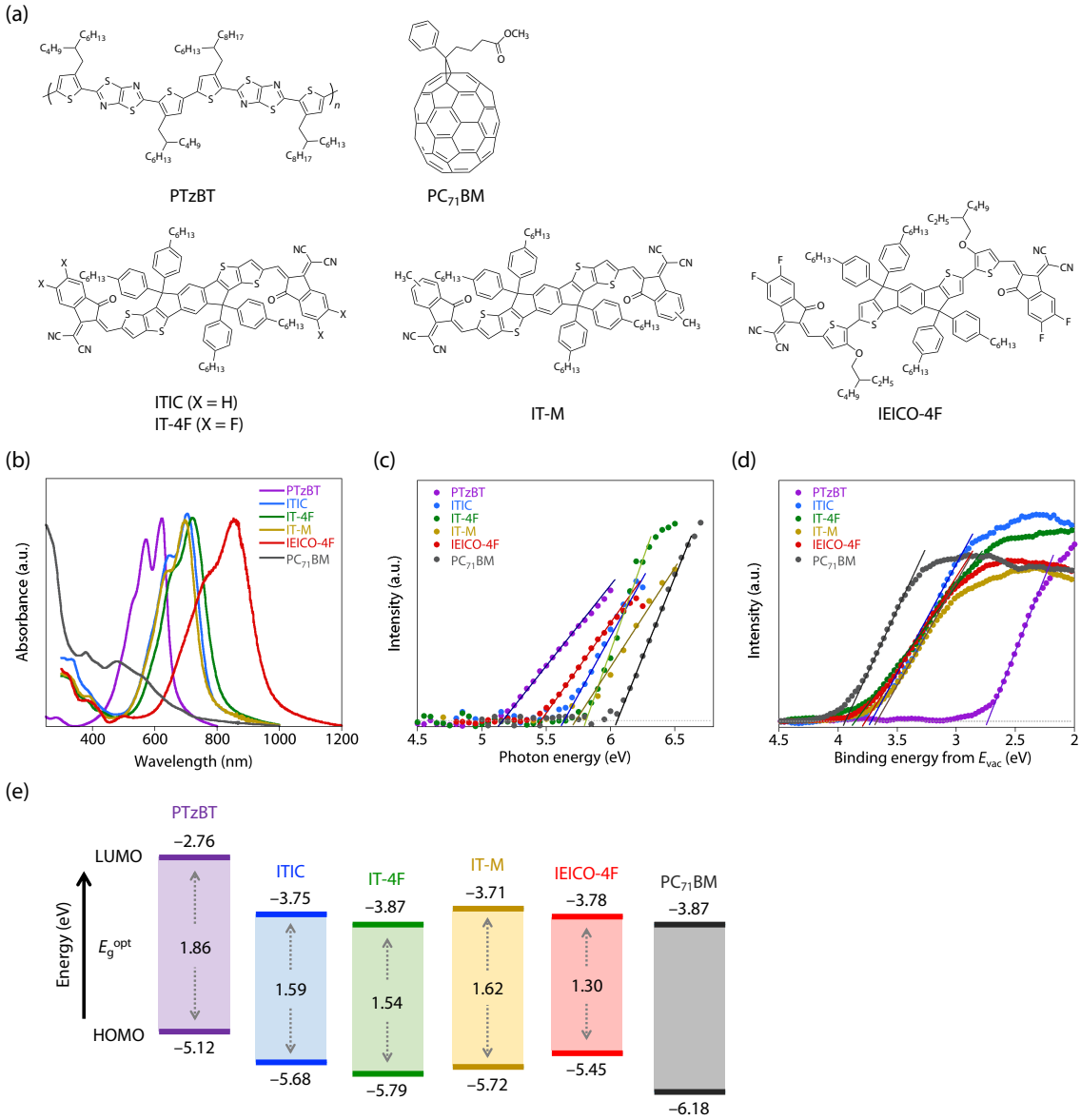

Figure 1. (a) Chemical structures, (b) UV–vis absorption spectra, (c) photoelectron yield spectra, (d) low-energy inverse photoelectron spectra, and (e) energy diagrams for the materials used in this study. HOMO and LUMO energy levels were determined from photoelectron yield spectra and low-energy inverse photoelectron spectra. All the spectra (a–c) were measured in thin films.

RESULTS AND DISCUSSION

Materials properties

Figure 1b shows the UV–vis absorption spectra for PTzBT, $PC_{71}BM$, and NFAs (ITIC, IT-4F, IT-M, and IEICO-4F). As previously reported, PTzBT showed a relatively narrow absorption spectrum covering 400–700 nm and had an absorption maximum (λ_{max}) at 622 nm and an absorption edge (λ_{edge}) at 680 nm, which corresponds to the optical bandgap (E_g^{opt}) of 1.86 eV. $PC_{71}BM$ had a strong absorption peak at around 350 nm and a shoulder that extended to around 600 nm. ITIC, IT-4F, and IT-M gave absorption spectra covering 500–800 nm with λ_{edge} at 780 nm, 805 nm, and 760 nm corresponding to the E_g^{opt} of 1.59 eV, 1.54 eV, and 1.62 eV, respectively, whereas IEICO-4F showed further red-shifted absorption in the range of 600–950 nm with λ_{edge} at 954 nm and thus the E_g^{opt} of 1.30 eV. Therefore, the addition of NFAs to the PTzBT/$PC_{71}BM$ host system results in an increase of the absorption range, thereby harvesting photons over almost the entire visible spectral range.

The highest occupied molecular orbital (HOMO) and lowest unoccupied molecular orbital (LUMO) energy levels (E_{HOMO} and E_{LUMO}) of the materials were determined in the solid state by photoelectron yield spectroscopy (PYS) (**Figure 1c**) and low-energy inverse photoelectron spectroscopy (LEIPS)[52-53] (**Figure 1d**), respectively, and are summarized as energy diagrams (**Figure 1e**). The E_{HOMO} and E_{LUMO} were −5.12 eV and −2.76 eV for PTzBT, and −6.18 eV and −3.87 eV for $PC_{71}BM$, respectively. The E_{HOMO} and E_{LUMO} were −5.68 eV and −3.75 eV for ITIC, −5.79 eV and −3.87 eV for IT-4F, −5.72 eV and −3.71 eV for IT-M, and −5.45 eV and −3.78 eV for IEICO-4F, respectively. All these values were mostly in between those of PTzBT and $PC_{71}BM$, indicating that the energy levels in these ternary blend systems were nearly cascaded. Note that the E_{HOMO} and E_{LUMO} of the materials were also evaluated by cyclic voltammetry (**Figure S1**, **Table S1**), and the trend was similar to those determined by PYS and LEIPS.

Solar cell performances

We first fabricated binary blend cells with an inverted structure (ITO/ZnO/photoactive layer/MoO_x/Ag) using the PTzBT/$PC_{71}BM$ (1:2 w/w) and PTzBT/ITIC (1:1.5 w/w) blend films as the photoactive layer. The EQE spectra and the current density (J)–voltage (V) curves for the cells are displayed in **Figures 2a** and **2b**, respectively, and the photovoltaic parameters are summarized in **Table 1**. The PTzBT/$PC_{71}BM$ cell exhibited as high as 7.4% PCE with a J_{SC} of 11.8 mA cm^{-2}, a V_{OC} of 0.88 V, and an FF of 0.71, consistent with the results reported previously.[21,23] The relatively small J_{SC} was due to the limited absorption range of up to ca. 670 nm, which corresponds to the absorption of PTzBT. A striking feature of the cell was that the optimal photoactive layer thickness was more than 300 nm, which is very thick for OPVs. This most likely originated in the high crystallinity and the face-on orientation of the polymer in the $PC_{71}BM$-blend film. With respect to the PTzBT/ITIC binary blend cell, although this cell had a wider spectral response than the PTzBT/$PC_{71}BM$ binary blend cell, it gave a modest J_{SC} of 11.7 mA cm^{-2} because of the relatively low EQE values throughout the absorption range. It was also unfortunate that the cell exhibited a low FF of 0.61 even when the photoactive layer was as thin as 120 nm, which was the optimal thickness. Thus, the PCE was limited to 7.1%. In contrast to the PTzBT/$PC_{71}BM$ cell, the performance of the cell severely deteriorated when the photoactive layer was thicker (**Figure S2**, **Table S2**). This can be explained by the low crystallinity of the polymer when blended with ITIC (**Figure S3**). Notably, however, the E_{loss} that is defined as $E_g^{opt} - eV_{OC}$[54-57] was 0.62 eV for the PTzBT/ITIC cell, which was significantly small relative to 0.98 eV for the PTzBT/$PC_{71}BM$ cell. In addition, we also fabricated an ITIC/$PC_{71}BM$ cell. However, it showed almost no photovoltaic response (**Figure S4**), most likely due to the extremely small offset energy of the E_{LUMO} (ΔE_L) between ITIC and $PC_{71}BM$, which is a simple measure of the driving force energy for the charge separation.

We then fabricated ternary blend cells using the PTzBT/$PC_{71}BM$ (1:2 w/w) blend as the host binary system and ITIC as the third component. We first optimized the content of ITIC while the

PTzBT/$PC_{71}BM$ weight ratio was set to 1:2. **Figures 3a** and **3b** depict the EQE spectra and the *J*–*V* curves for the ternary blend cells with an ITIC ratio of 0 to 40 wt%. By the addition of 3 wt% ITIC (PTzBT:$PC_{71}BM$:ITIC = 1:2:0.1), the absorption range was expanded to ca. 770 nm and the EQE at 700 nm was 28% (**Figure 3a**). This indicates a clear contribution of ITIC to the photoconversion even though the ITIC content is very small. Surprisingly, increasing the ITIC content to 6 wt% (PTzBT:$PC_{71}BM$:ITIC = 1:2:0.2) significantly boosted the EQE at around 700 nm to 66%, which was comparable to that in the PTzBT absorption range (EQE = 67% at 620 nm). Note that the weight ratio of ITIC to PTzBT was only one-fifth. However, it is interesting that the further increase in ITIC content of up to 40 wt% gradually decreased the EQE at around 700 nm to 40%, which was also accompanied by a significant decrease in the EQE in the PTzBT absorption range. Accordingly, J_{SC} was maximized at the ITIC content of 6 wt% and decreased with further increase in the ratio (**Figure 3b**, **Table 2**).

The V_{OC} for the ternary blend cell with the small ITIC content (3–9 wt%) was 0.89 V, which was almost the same as that for the PTzBT/$PC_{71}BM$ binary blend cell (**Figure 3b**, **Table 2**). Increasing the ITIC content, however, increased V_{OC}, and V_{OC} was 0.94 V at the ITIC content of 40 wt%. This is consistent with the fact that the PTzBT/ITIC system gave a higher V_{OC} than the PTzBT/$PC_{71}BM$ system. Importantly, E_{loss} for the PTzBT/$PC_{71}BM$/ITIC ternary blend cell was significantly reduced to 0.70 eV at the ITIC content of 3–9 wt% relative to that for the PTzBT/$PC_{71}BM$ binary blend cell of 0.98 eV. This originated in the difference in the bandgap between the ternary and the binary systems, where the former was determined by ITIC (1.59 eV) and the latter was determined by PTzBT (1.86 eV), whereas V_{OC} was almost the same for both systems. The ternary blend cell with the ITIC content of 40 wt% showed the minimum E_{loss} of 0.65 eV for this system.

The FF for the ternary blend cell with the ITIC content of 3–14 wt% was 0.70–0.71, which was almost the same as that for the PTzBT/$PC_{71}BM$ binary blend cell (**Table 2**). However, a further increase in the ITIC content was detrimental as was seen from the lower FF for the PTzBT/ITIC cell than the PTzBT/$PC_{71}BM$ cell. As a result, PCE for the ternary blend cell was maximum at 10.3% at the ITIC

ratio of 6 wt% (J_{SC} = 16.5 mA cm^{-2}, V_{OC} = 0.89 V, FF = 0.70). It is important to note that the optimal thickness for the photoactive layer was 360 nm (**Figure 3**, **Table 3**), as is the case for the PTzBT/$PC_{71}BM$ cell. In addition, the use of $PC_{61}BM$ instead of $PC_{71}BM$ gave similar results (**Figure S5**, **Table S3**).

We also tested the sensitized ternary blend cells by using other NFAs, such as IT-4F, IT-M, and IEICO-4F, as the third component. **Figures 2c** and **2d** depict the EQE spectra and the *J*–*V* curves for the cells with the optimal NFA content of 6 wt%, and **Table 1** summarizes the photovoltaic parameters. All these ternary blend cells showed higher PCEs than the binary blend cells that used PTzBT and the corresponding NFAs (**Figure S6**, **Table 1**) as well as the PTzBT/$PC_{71}BM$ cell. Notably, the optimal thickness of all these systems was also around 300 nm. The PTzBT/$PC_{71}BM$/IT-4F cell showed reasonably high photovoltaic performance with a PCE of 9.9% (J_{SC} = 15.6 mA cm^{-2}, V_{OC} = 0.85 V, FF = 0.70), although V_{OC} was lower than that for the ITIC ternary blend cell, resulting in the E_{loss} of 0.73 eV. The low V_{OC} is most likely a result of the deeper E_{LUMO} for IT-4F than ITIC. On the other hand, the PTzBT/$PC_{71}BM$/IT-M cell showed a high V_{OC} of 0.92 V owing to the shallow E_{LUMO} of IT-M relative to that of ITIC and IT-4F, although E_{loss} was almost the same as that for the ITIC and IT-4F cells due to the slightly wider E_g^{opt} for IT-M. In addition, PCE was limited to 9.4% due to the smaller J_{SC}, which in part originated in the slightly wider E_g^{opt} for IT-M than ITIC. Although the overall performance of these cells was lower than that of the ITIC cell, these results suggested that the energetics of the third component affects V_{OC}, and thus the choice of materials with more suitable energetics, including E_g^{opt}, can further enhance the performance of the ternary blend cell.

In the IEICO-4F ternary blend cell, the EQE spectrum covered the absorption range of up to approximately 950 nm, although the EQE values were not as high as those for the ternary blend cells that used ITIC, IT-4F, and IT-M. Nevertheless, the IEICO-4F ternary blend cell had a J_{SC} of 16.9 mA cm^{-2}, which was larger than that for the other ternary blend cells. Notably, it showed a V_{OC} of 0.83 V, which was lower than that for the PTzBT/$PC_{71}BM$ cell but higher than that for the PTzBT/IEICO-4F

cell, contrary to our expectations based on the difference in E_{LUMO}. In fact, this trend was opposite to the case for the other NFAs, where the PTzBT/NFA binary blend cells that used ITIC, IT-4F, and IT-M showed higher V_{OC} than the PTzBT/$PC_{71}BM$ cell as well as the corresponding ternary blend cell. Although we do not know the reason so far, the energetics might differ when the materials are blended due to intermolecular interactions at the interface. Consequently, E_{loss} was significantly reduced to 0.47 eV, which was even smaller than 0.52 eV for the PTzBT/IEICO-4F cell, with a relatively high PCE of 8.9% for OPVs with such a small E_{loss}.[51,58-61]

In order to better complement the absorption range, we fabricated a quaternary cell based on the PTzBT/$PC_{71}BM$ binary system with small amounts of ITIC and IEICO-4F, where the optimal content for ITIC and IEICO-4F was found to be 3 wt% each. The optimal photoactive layer thickness was 280 nm. Although the EQE values in the absorption range for the two NFAs were low relative to those for the corresponding ternary blend cells due to the low content (**Figure 2c**), and thus J_{SC} was small (**Figure 2d**), ITIC successfully buried the valley between PTzBT and IEICO-4F absorptions. It is interesting that V_{OC} slightly increased to 0.85 V compared to that for the IEICO-4F ternary blend cell (**Table 1**), most likely owing to the addition of ITIC with E_{LUMO} shallower than that for IEICO-4F. Consequently, the quaternary cell had an E_{loss} of as small as 0.45 eV, considered one of the smallest values for OPVs, with an enhanced PCE of 9.3%.

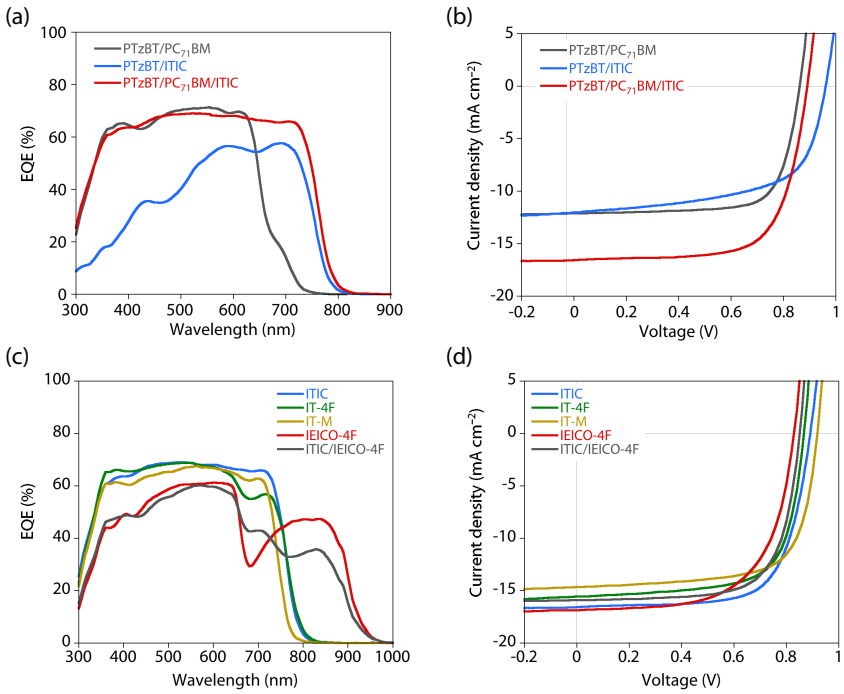

Figure 2. (a) EQE spectra and (b) *J*–*V* curves for photovoltaic cells based on PTzBT/$PC_{71}BM$ (1:2 w/w) and PTzBT/ITIC (1:1.5 w/w) binary blends, and PTzBT/$PC_{71}BM$/ITIC ternary blend with 6 wt% ITIC (1:2:0.2 w/w/w). (c) EQE spectra and (d) *J*–*V* curves for photovoltaic cells based on ternary blends that used PTzBT/$PC_{71}BM$ as the host binary blend and ITIC, IT-4F, IT-M, and IEICO-4F with 6 wt% as the third component, and the PTzBT/$PC_{71}BM$/ITIC/IEICO-4F quaternary blend with 3 wt% each for ITIC and IEICO-4F (1:2:0.1:0.1 w/w/w/w).

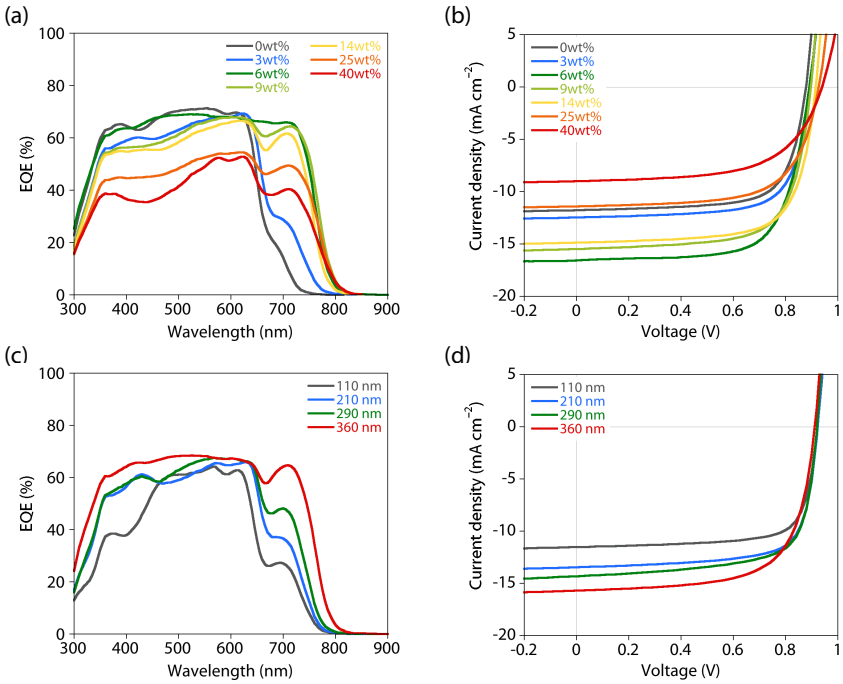

Figure 3. (a) EQE spectra and (b) *J*–*V* curves for photovoltaic cells based on the PTzBT/$PC_{71}BM$/ITIC blend with different ITIC contents (0–40 wt%). (c) EQE spectra and (d) *J*–*V* curves for photovoltaic cells based on the PTzBT/$PC_{71}BM$/ITIC blend (6 wt%) with different photoactive layer thicknesses (110, 210, 290, and 360 nm).

Table 1. Photovoltaic parameters of cells based on PTzBT/$PC_{71}BM$ and PTzBT/ITIC binary blends and PTzBT/$PC_{71}BM$/ITIC ternary blend.

Photoactive layer	Thickness (nm)[c]	J_{SC} (mA cm^{-2})	V_{OC} (V)	FF	PCE (%)[d]	E_{loss} (eV)[e]
PTzBT/$PC_{71}BM$	340	11.8	0.88	0.71	7.4	0.98
PTzBT/ITIC	120	11.7	0.97	0.61	7.1	0.62
PTzBT/$PC_{71}BM$/ITIC[a]	350	16.5	0.89	0.70	10.3	0.70
PTzBT/IT-4F	140	10.0	0.90	0.72	6.4	0.64
PTzBT/$PC_{71}BM$/IT-4F[a]	320	15.6	0.85	0.70	9.9	0.73
PTzBT/IT-M	110	11.8	1.00	0.64	7.6	0.63
PTzBT/$PC_{71}BM$/IT-M[a]	300	14.7	0.92	0.70	9.4	0.71
PTzBT/IEICO-4F	120	7.0	0.78	0.40	2.2	0.52
PTzBT/$PC_{71}BM$/IEICO-4F[a]	300	16.9	0.83	0.64	8.9	0.47
PTzBT/$PC_{71}BM$/ITIC/IEICO-4F[b]	280	15.6	0.85	0.70	9.3	0.45

a) 6 wt% of NFA was used (PTzBT:$PC_{71}BM$:NFA = 1:2:0.2). b) 3 wt% of ITIC and IEICO-4F was used (PTzBT:$PC_{71}BM$:ITIC:IEICO-4F = 1:2:0.1:0.1). c) Optimal photoactive layer thickness. d) Maximum power conversion efficiency. e) Photon energy loss: $E_g^{opt} - eV_{OC}$.

Table 2. Photovoltaic parameters of cells based on PTzBT/$PC_{71}BM$/ITIC ternary blend with different ITIC contents.

ITIC content (wt%)	Thickness (nm)	J_{SC} (mA cm^{-2})	V_{OC} (V)	FF	PCE (%)
0	340	11.8	0.88	0.71	7.4
3	330	12.5	0.89	0.71	7.9
6	350	16.5	0.89	0.70	10.3
9	350	15.5	0.89	0.70	9.7
14	330	14.9	0.91	0.71	9.6
25	360	11.4	0.93	0.66	7.0
40	350	9.0	0.94	0.61	5.1

Table 3. Photovoltaic parameters of cells based on PTzBT/$PC_{71}BM$/ITIC (6 wt%) ternary blend with different photoactive layer thicknesses.

Thickness (nm)	J_{SC} (mA cm^{-2})	V_{OC} (V)	FF	PCE (%)
110 nm	11.5	0.91	0.75	7.9
210 nm	13.5	0.91	0.73	9.1
290 nm	14.3	0.91	0.70	9.3
360 nm	16.5	0.89	0.70	10.3

Optical measurements and simulations

As described above, in the PTzBT/$PC_{71}BM$/ITIC ternary blend cell, EQE in the ITIC absorption range was as high as that in the polymer absorption range, particularly in the cell with a thick photoactive layer, despite the fact that the ITIC content is only 6 wt%. We thus first examined the absorption efficiency for the ternary blend film (1:2:0.2 w/w/w; ITIC 6 wt%) by measuring the UV–vis absorption spectra in both the normal mode using transmitted light and the reflection mode, and compared them with those for the PTzBT/ITIC (1:1.5 w/w) binary blend film (**Figure 4a**). Note that the thickness of the ternary and binary blend films was set to the optimal value for each solar cell; approximately 340 nm for the ternary blend film and 120 nm for the binary blend film. It was found that in the normal mode, the absorption efficiency for the ITIC band in the ternary blend film was only 24%, reflecting the ITIC content. This was far lower than that for the PTzBT band (86%) in the same film, and was also far lower than that for the ITIC band in the PTzBT/ITIC binary blend film (73%). However, in the reflection mode, the absorption efficiency for the ITIC band in the ternary blend film was significantly increased to 81%, which was close to that for the PTzBT band (93%) in the same film as well as that for the ITIC band in the binary blend film (89%). We also note that the absorption efficiency for the ITIC band with respect to the PTzBT band in the ternary blend was significantly higher in the thicker film than the thinner film (**Figure 4b**). This was also the case in the PTzBT/$PC_{71}BM$/IEICO-4F film having broader absorption in the long-wavelength range (**Figure S7**), and was in good agreement with the photovoltaic properties (**Figure S8**, **Table S4**).

To study this effect further, we then simulated the distribution of light absorption within the ternary blend film on the cell.[62] We first carried out variable angle spectroscopic ellipsometry (VASE) measurements to determine the refractive indices and the extinction coefficients for the PTzBT/$PC_{71}BM$/ITIC (6 wt%) film (**Figure S9a**) as well as the materials used for the photovoltaic cell, such as glass, ITO, ZnO, and MoO_x (**Figure S9b**). Using these optical constants, we performed a simulation of the reflection absorption spectra for the ternary blend films (**Figure S10**), and found that

the simulated spectra nicely reproduced the experimental data shown in **Figure 4b**. **Figure 4c** displays the simulated absorption distribution inside the cells with the wavelength (horizontal axis) and the distance from the interface between the ZnO layer and the photoactive layer (vertical axis) to the Ag electrode with different photoactive layer thicknesses. Note that the thickness values for the ternary blend films shown here were determined by the VASE measurement and thus were slightly different from the values measured by a profilometer, particularly for the thick film: 120, 180, 280, and 430 nm by the VASE measurement corresponded to 110, 210, 290, and 360 nm measured by the profilometer. In the thin films with 120 and 180 nm thickness, there was only one maximum for the absorption at around 700 nm, which corresponded to the ITIC absorption band, within the photoactive layer. When the thickness was increased to 280 and 430 nm, we observed two and three maxima for the same ITIC absorption band, respectively. The result indicates that there is clear optical interference effect in the ITIC absorption band. In fact, the plot of the simulated absorption efficiency at 700 nm vs. photoactive layer thickness shown in **Figure 4d** showed a strong multiple-intensity oscillation, in which the absorption efficiency gradually increased with three maxima as the thickness increased, resulting in the highest absorption efficiency around the thickness of 400 nm. The fact that the optical interference effect significantly appeared for ITIC even though its concentration was very low is very interesting. On the other hand, in the film with 180 nm thickness, the absorption band around 400–650 nm wavelength corresponding to the PTzBT band had two maxima within the layer, which was also indicative of the optical interference effect. However, in the thicker films (280 and 430 nm), this optical interference effect was absent for the PTzBT band as there was only one maximum that was located around the ZnO/photoactive layer interface. Thus, the absorption by PTzBT at 620 nm wavelength was saturated at the thickness of ~200 nm (**Figure 4d**). Considering the different absorption behavior between ITIC and PTzBT, the well-dispersed ITIC at a low concentration would account for the observation of the multiple absorption maxima in the ternary film. This simulated absorption distribution is in good agreement with the fact that the absorption efficiency for the ITIC band

significantly increased with the increase in thickness, and the EQE value for the ITIC band was markedly high even though the ITIC content was very low.

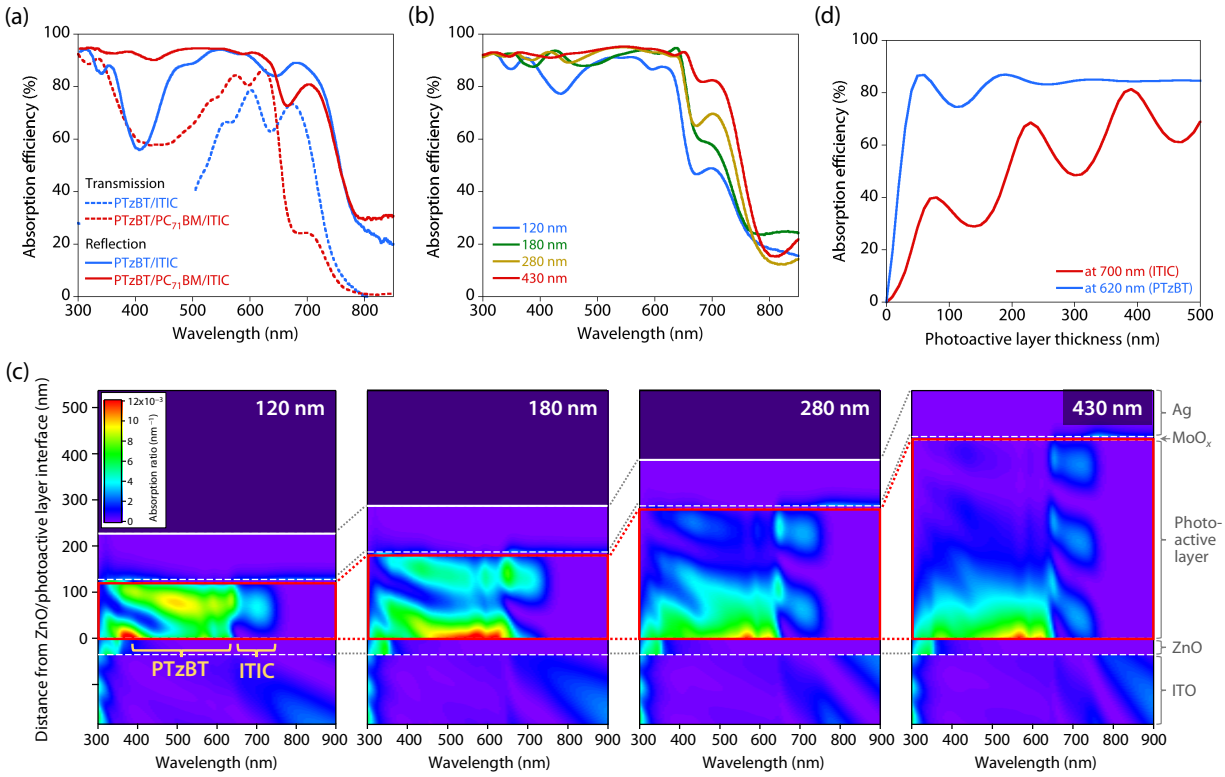

Figure 4. (a) UV–vis absorption spectra for PTzBT/ITIC and PTzBT/PC_{71}BM/ITIC (6 wt%) films in the normal and reflection modes. (b) UV–vis absorption spectra for the PTzBT/PC_{71}BM/ITIC (6 wt%) film in the reflection mode with different thicknesses. Note that the thickness was measured by VASE measurement: 110, 180, 280, and 430 nm correspond to the thicknesses of 110, 210, 290, and 360 nm measured by a profilometer, respectively. (c) Simulated absorption distribution for the PTzBT/PC_{71}BM/ITIC (6 wt%) cells with different photoactive layer thicknesses. (d) Simulated absorption efficiency for the PTzBT/PC_{71}BM/ITIC (6 wt%) film at 620 nm (PTzBT) and 700 nm (ITIC) as a function of photoactive layer thickness.

Distribution of three components and working mechanism in the ternary blend system

In the sensitized ternary blend cells, as the content of the third component is very small, the distribution (location) of the three components plays an important role.[38,41] It was reported that in the sensitized ternary blend system based on the P3HT/$PC_{61}BM$ host binary system with a phthalocyanine derivative as the third component, the phthalocyanine molecules were selectively located at the interface between the P3HT and $PC_{61}BM$ domains.[40] We thus discuss here how the three components are distributed in the present system by the grazing incidence X-ray diffraction (GIXD) measurements as well as the transient absorption spectroscopy (TAS) and contact angle measurement.[40-41,63] Note that in these measurements, $PC_{61}BM$ was used instead of $PC_{71}BM$ because the trend in the OPV performance of these fullerenes was almost the same.

GIXD study

Figure 5a depicts the two-dimensional (2D) GIXD patterns of the PTzBT/$PC_{61}BM$/ITIC ternary blend films with different ITIC contents (0, 3, 6, 9, 14, 25, and 40 wt%). Diffraction profiles along the quasi-q_z and q_{xy} axes cut from the 2D patterns are also depicted in **Figure S11**. As previously reported, at 0 wt% ITIC, i.e., the PTzBT/$PC_{61}BM$ binary blend film, PTzBT showed clear diffractions corresponding to the lamellar structure, (h00), along both quasi-q_z and q_{xy} axes (q = 0.31 $Å^{-1}$) and a diffraction corresponding to the π–π stacking structure, (010), along the quasi-q_z axis (q = 1.80 $Å^{-1}$), indicating that the polymer assumed face-on orientation. Furthermore, these diffractions were relatively sharp for semiconducting polymers, which suggested that PTzBT had high crystalline nature. In fact, the d-spacing for the π–π stacking structures (d_π) was 3.48 Å, which was significantly small, and the d-spacing for the lamellar structure (d_L) was approximately 20 Å. The diffuse ring at q = 1.31 $Å^{-1}$ corresponds to the aggregation of $PC_{61}BM$ with the d-spacing (d_{PCBM}) of 4.7 Å. When ITIC was added, the 2D GIXD pattern did not change, suggesting that the crystalline structures of the polymer and $PC_{61}BM$ were preserved. It is noted that the diffractions for ITIC were not observed in these

patterns even when relatively large amounts, such as >25 wt%, were added (see **Figure S3** for the 2D GIXD pattern of ITIC neat film).

Figure 5b (upper) shows the change in *d*-spacings as a function of the ITIC content. When the ITIC content was increased, although d_L almost did not change, d_π slightly but gradually enlarged to 3.55Å at 40 wt%. With respect to $PC_{61}BM$, d_{PCBM} gradually decreased to 4.5 Å, implying that the aggregates became smaller. We also calculated the coherence lengths for the three structural orders, i.e., lamella (L_L), π–π stacking (L_π), and $PC_{61}BM$ (L_{PCBM}), using the simplified Scherrer's equation (2π/FWHM: FWHM = full width at half-maximum of the diffraction peak).[64] **Figure 5b** (lower) shows the dependence of L_L, L_π, and L_{PCBM} on the ITIC content. It is clear that at larger ITIC contents, the coherence length decreased for all the structural orders. These results imply that at smaller ITIC contents, the PTzBT and $PC_{61}BM$ domains remained pure and the ITIC molecules should be isolated from both domains, being located at the interface between the PTzBT and $PC_{61}BM$ domains and/or in the amorphous phase. As changes in the *d*-spacings for all the structural orders were marginal, although d_π did increase to some extent, the ITIC molecules were not likely to penetrate either the PTzBT or $PC_{61}BM$ domain even at larger contents. Nevertheless, the addition of large amounts of ITIC was detrimental to the crystallinity for both PTzBT and $PC_{61}BM$, consistent with the lower photovoltaic performance, as well as the hole mobility (**Figure S12**, **Table S5**), in the larger ITIC contents. In addition, the transmission electron microscopy (TEM) also revealed that when the ITIC content was small, the morphology for the PTzBT/$PC_{61}BM$/ITIC ternary blend was almost the same as that for the PTzBT/$PC_{61}BM$ binary blend. However, the morphology for the ternary blend was significantly changed when the ITIC was increased, in particular for more than 25 wt% (**Figure S13**). This is consistent with the change in the crystallinity by 2D GIXD measurements, and thus the hole mobility and photovoltaic performance.

Transient absorption spectroscopy

We measured the time evolution of the transient absorption spectra for the PTzBT/$PC_{61}BM$/ITIC

film with the ITIC content of 6 wt% within the picosecond time range (~3000 ps). First, the film was photoexcited at 700 nm, where ITIC was selectively excited (**Figure 5c**). Immediately after the laser excitation (0 ps), a transient absorption band was observed at around 850–1050 nm, which was assigned to the ITIC singlet exciton by taking into account the transient absorption spectra for the PTzBT/ITIC film photoexcited at 700 nm (**Figure S13a**). **Figure 5d** shows the decay of the ITIC singlet and PTzBT ground state bleach (GSB) that was observed at around 500–680 nm. The ITIC singlet exciton then decayed with the time constant of 7 ps, which, importantly, was almost the same as that for the rise of the PTzBT GSB signal. This suggests that the hole transfer from ITIC to PTzBT occurred and thus these two materials should contact each other. Accordingly, we observed an absorption band assignable to the PTzBT polaron (hole generated on PTzBT), which had a peak at ca. 980 nm and thus was mostly overlapped with the ITIC singlet exciton band: the peak of the absorption in 850–1050 nm gradually red-shifted from 950 to 980 nm with time, which indicated that the population of the ITIC singlet exciton decreased and, at the same time, the population of the PTzBT polaron increased. In addition, the fact that the ITIC singlet exciton decayed slowly in the time scale of several picoseconds suggests that ITIC formed some aggregates in the ternary blend.

The film was then photoexcited at 500 nm, where PTzBT was selectively excited (**Figure 5e**). A transient absorption band was observed at around 1050–1500 nm immediately, which was assigned to the PTzBT singlet exciton by considering the transient absorption spectra for the PTzBT/$PC_{61}BM$ film photoexcited at 500 nm (**Figure S13b**). Interestingly, the ITIC singlet exciton band was also observed at 0 ps, which further intensified with a similar time scale to the decay of the PTzBT singlet exciton. This suggests that there was an energy transfer from PTzBT to ITIC. The PTzBT polaron was also observed similarly to the case of the photoexcitation at 700 nm. It goes without saying that the generation of the PTzBT polaron suggests that the electron transfer from PTzBT to either $PC_{61}BM$ or ITIC, or both, occurred. However, it should be noted that considering the amount of the materials included in the ternary blend, electron transfer from PTzBT to $PC_{61}BM$ certainly occurred.

Figure 5f shows the transient absorption spectra for the PTzBT/$PC_{61}BM$, PTzBT/ITIC, and PTzBT/$PC_{61}BM$/ITIC films 1000 ps after the PTzBT excitation at 500 nm. The absorption in the range of approximately 650–800 nm also corresponds to the PTzBT polaron. Further, in the case of the PTzBT/ITIC and PTzBT/$PC_{61}BM$/ITIC films, this signal overlapped with the GSB of ITIC. Thus, comparison of these spectra would allow us to discuss the generation of anions, i.e., to which material the electron transfer from PTzBT occurred. Note that the transient absorption bands for the anions could not be observed directly due to the extremely low intensity of the signals. The spectra for the PTzBT/$PC_{61}BM$ and PTzBT/ITIC films represent the states in which the anions reside on $PC_{61}BM$ and ITIC, respectively. With respect to the PTzBT/$PC_{61}BM$/ITIC film, its spectrum appeared to be a superposition of the spectra for both the binary films. This suggests that the anions in the ternary blend film reside on both $PC_{61}BM$ and ITIC. Thus, it is most likely that electron transfer occurred from PTzBT to both $PC_{61}BM$ and ITIC, meaning that PTzBT should contact both $PC_{61}BM$ and ITIC.

Materials distribution and working mechanism

In this ternary blend, both PTzBT and $PC_{61}BM$ formed crystalline domains similarly to the PTzBT/$PC_{61}BM$ binary blend, in particular when the ITIC content was small, as the 2D GIXD patterns for the binary and the ternary blends were almost the same. Thus, we conclude that the ITIC molecules penetrated neither the PTzBT nor the $PC_{61}BM$ domain. As suggested by TAS, ITIC likely formed aggregates, but perhaps the aggregates were small considering the amount of ITIC added into the ternary blend. Furthermore, TAS confirmed that PTzBT had contact with both $PC_{61}BM$ and ITIC. It is also noted that if the ITIC molecules had penetrated the PTzBT domain, the generated electrons would not be extracted because of the disconnected ITIC network. On the other hand, if there were ITIC molecules in the $PC_{61}BM$ domain, those molecules would not undergo charge separation as revealed by the fact that the ITIC/$PC_{61}BM$ cell did not work at all. Both cases are detrimental to the OPV performance of the ternary blend cell, which should not be the case here. Overall, the distribution of PTzBT, $PC_{61}BM$, and ITIC is most likely to be that illustrated in **Figure 5g**, in which the small ITIC

aggregates are mainly located at the interface of the PTzBT crystallites and $PC_{61}BM$ aggregates, where the PTzBT amorphous phases should also exist. We assume that this was driven by the highly crystalline nature of PTzBT.

Note that, however, the contact angle measurements revealed that the surface energy of $PC_{61}BM$ (33.3 mJ m^{-2}) was close to that of ITIC (31.2 mJ m^{-2}), while that of PTzBT was much smaller (27.1 mJ m^{-2}) (**Table S6**), implying that ITIC molecules are likely to mix with $PC_{61}BM$ molecules: this should also be the case when $PC_{71}BM$ is used since the surface energy for $PC_{71}BM$ (31.1 mJ m^{-2}) was similar. Thus, the $PC_{61}BM$ molecules could also co-exist with the ITIC molecules in the polymer amorphous regions. In addition, when the ITIC content is large, ITIC molecules can further mix with $PC_{61}BM$ molecules and thus they could penetrate into and destroy the $PC_{61}BM$ aggregates, which would also decrease the crystallinity of PTzBT.

Thus, the working mechanism of this ternary blend is explained as follows. When PTzBT absorbs incident light and generates excitons, electron transfer to both $PC_{61}BM$ and ITIC occurs, and energy transfer to ITIC occurs as well. The hole generated in PTzBT is transported through the PTzBT domain to the positive electrode. Excitons generated in ITIC upon light absorption are separated at only the PTzBT/ITIC interface because the ITIC/$PC_{61}BM$ binary blend did not show photoresponse (**Figure S4**). This is also the case when ITIC generates excitons by energy transfer from PTzBT. The electrons generated in ITIC are injected into $PC_{61}BM$, which helps the electrons sweep out to the negative electrode. The excitons generated in $PC_{61}BM$ are separated into free charges at the PTzBT interface by the hole transfer.

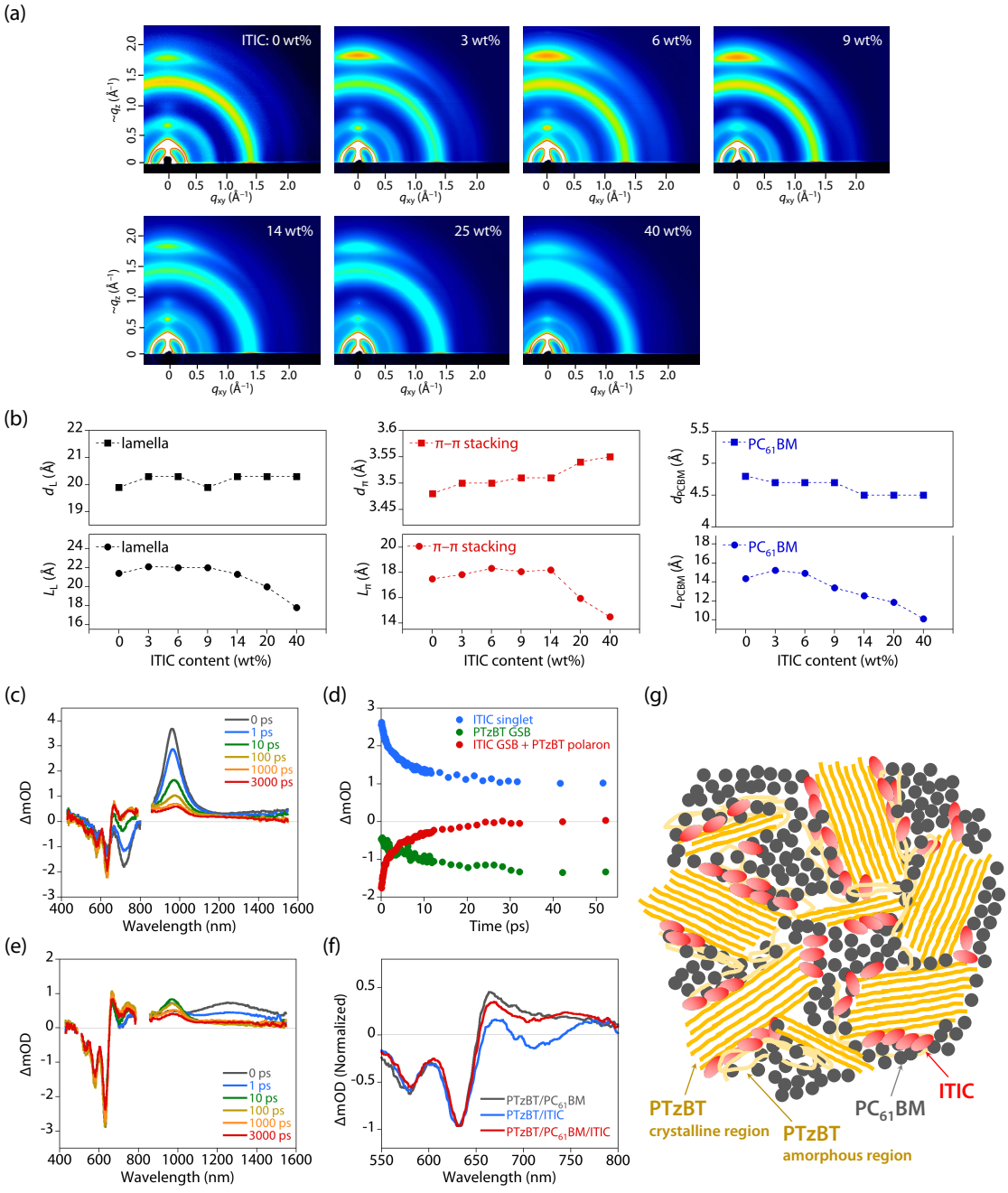

Figure 5. 2D GIXD and TAS studies to determine the distribution of the materials. (a) 2D GIXD patterns of PTzBT/$PC_{61}BM$/ITIC ternary blends with different ITIC contents (0–40 wt%). The ITIC content is shown on the top right of each pattern. (b) Dependence on the ITIC content of *d*-spacings (upper) and coherence length (lower) for the lamellar and π–π stacking orders of PTzBT and for the aggregate of $PC_{61}BM$. (c–f) Transient absorption spectra for the PTzBT/$PC_{61}BM$/ITIC (6 wt%) ternary blend film. (c) Spectra measured at 0–3000 ps after photoexcitation at 700 nm. (d) Change in signals for the ITIC singlet and PTzBT ground state bleach (GSB) over time. (e) Spectra measured at 0–3000 ps after photoexcitation at 500 nm. (d) Comparison of spectra, measured at 1000 ps after

photoexcitation at 500 nm, for the PTzBT/$PC_{61}BM$ and PTzBT/ITIC binary blend films. (g) Proposed schematic illustration of the distribution of materials in the ternary blend film.

Thermal stability of ternary blend cell

We studied the thermal stability of the cells based on the PTzBT/$PC_{71}BM$ binary blend and the PTzBT/$PC_{71}BM$/ITIC (6 wt%) ternary blend. The cells were heated at 85 °C in the dark under an N_2 atmosphere (glove box) for 1000 h.[65] The *J*–*V* characteristics were measured at room temperature. **Figure 6a** shows the relative changes in PCE as a function of storage time. Interestingly, the ternary blend cell showed markedly increased thermal stability under the above-mentioned conditions. The binary blend cell demonstrated a significant decrease in PCE to approximately 80 percent of the initial value within the initial 24 h. Then, its PCE further decreased to approximately 70 percent at 200 h and was maintained at this value up to 1000 h.[66-67] In contrast, the PCE of the ternary blend cell gradually decreased to approximately 90 percent of the initial value at 200 h and was maintained at this value up to 1000 h. The difference was largely due to the difference in FF (**Figure S14**). In addition, PTzBT/ITIC was also tested under the same conditions, but it significantly degraded within the initial 100 h (**Figure S15**). We further investigated the film structure by conducting 2D GIXD measurements (**Figure S16**). Whereas the d_π increased and the L_π declined for PTzBT in the binary blend after annealing the film at 85 °C, both d_π and L_π were unchanged for PTzBT in the ternary blend (**Figure 6b**). Thus, we assume that the morphology was significantly stabilized by the addition of ITIC, which seemed to account for the improved thermal stability of the ternary blend cell.

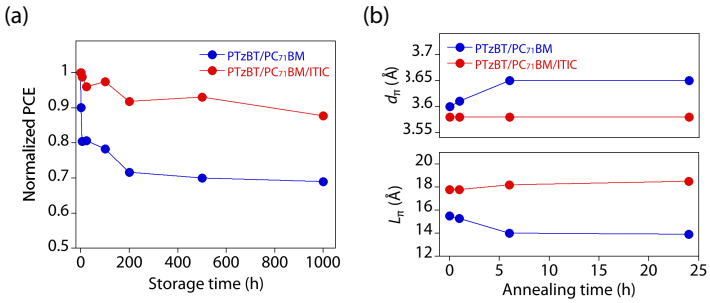

Figure 6. (a) Relative changes in PCE by storing the PTzBT/$PC_{71}BM$ binary blend cell and the PTzBT/$PC_{71}BM$/ITIC (6 wt%) ternary blend cell at 85 °C in the dark in a glove box for 1000 h. (b) Changes in d_π (upper) and L_π (lower) for PTzBT with annealing time for the PTzBT/$PC_{71}BM$ binary blend film and the PTzBT/$PC_{71}BM$/ITIC (6 wt%) ternary blend film.

CONCLUSIONS

In this work, we fabricated sensitized ternary blend cells that used crystalline polymer PTzBT and $PC_{71}BM$ as host donor and acceptor materials and a small amount of an NFA, such as ITIC, IT-4F, IT-M, or IEICO-4F, as the third component. Apparently, the NFA molecules were selectively located at the interface between the PTzBT and $PC_{71}BM$ domains as revealed by 2D GIXD and TAS measurements. The ternary blend cell with the ITIC content of 6 wt% demonstrated vastly improved PCE of over 10%, compared with the PTzBT/$PC_{71}BM$ binary blend cell that had a PCE of 7.4%. In addition, the ternary blend cell showed significantly reduced E_{loss} relative to the binary blend cell. Specifically, when IEICO-4F having a narrower bandgap than the other NFAs was used, E_{loss} was as small as 0.47 eV, which was smaller than that for the corresponding binary blend cell combined with PTzBT, unlike the case of the other NFAs, and was one of the smallest values for OPVs. Importantly, for all the NFAs, maximum performance was achieved with a very thick photoactive layer of more than 300 nm. We would like to stress that despite the fact that the NFA sensitizer content was very small, the EQE in the NFA absorption range, particularly for the cases of ITIC, IT-4F, and IT-M, was as high as that in the host polymer absorption range. This originated in the optical interference effect where the sensitizer absorption significantly intensified when the reflection at the back contact was taken into account. In fact, the optical simulation based on VASE measurements showed that multiple intensity maxima were observed in the NFA absorption range within the photoactive layer particularly when the layer thickness was increased. It is interesting to note that in the thick film, PTzBT absorbs most of the incident light within the first 100 nm thickness from the ZnO layer, whereas NFA (ITIC) absorbs the incident light throughout the film thickness. Thus, PTzBT carries generated holes to the Ag electrode over a distance of more than 300 nm distance, but still has high FF in excess of 0.7. This originates in the highly crystalline order and the high hole mobility of PTzBT, that is, the use of highly crystalline polymer as the host donor is essential for the sensitized ternary blend cells.

To the best of our knowledge, we showed for the first time that the sensitized ternary blend cell can function with a crystalline semiconducting polymer other than P3HT as the host donor. The presented

ternary blend cells require only a small amount of the third component that fully harvests incident photons in the corresponding absorption range by utilizing the optical interference effect, owing to the highly crystalline host polymer enabling a thick photoactive layer. Although it was shown by theoretical simulation that the combination of a narrow-bandgap donor polymer and a wide-bandgap sensitizer is desirable for such sensitized ternary blend cells, our results demonstrate that the opposite combination, a wide-bandgap donor polymer and a narrow-bandgap sensitizer, can be the better choice. In parallel, this type of ternary blend cells can realize significantly small E_{loss} and thus a high photovoltage, simultaneously with a large photocurrent. All these features are indeed important for improving PCE. In addition, the ternary blend cell significantly increased thermal stability compared with the binary blend cell. Although the overall PCE is still around 10%, we believe that the sensitized ternary blend cells show exceptional possibilities. Exploring more highly matched material combinations in terms of bandgap, energetics, and crystallinity as well as designing the optical interference would certainly improve the performance further.

EXPERIMENTAL SECTION

Materials. PTzBT,[21,68] ITIC,[48] IT-4F,[49] IT-M,[50] and IEICO-4F[51] were synthesized according to published procedures. $PC_{61}BM$ and $PC_{71}BM$ were purchased from Solenne BV.

Solar Cell Fabrication and Measurement. ITO substrates were first pre-cleaned sequentially by sonicating in a detergent bath, de-ionized water, acetone, and isopropanol at room temperature, and in boiled isopropanol each for 10 min, and then baked at 120 °C for 10 min in air. After that, the substrates were subjected to UV/ozone treatment at room temperature for 20 min. A ZnO layer was prepared by spin coating (at 1500 rpm) from a diluted solution of ZnO nanoparticles. The photoactive layer was deposited in a glove box (Korea Kiyon, KK-011AS-EXTRA) by spin coating a chlorobenzene solution of the blends (approximately 4–6 g L^{-1} concentration based on the polymer) at 600 rpm for 20 s, in which the solution was kept heated at 100 °C. The thin films were transferred into a vacuum evaporator (ALS Technology, E-100J) connected to the glove box. MoO_x (7.5 nm) and Ag (100 nm) were deposited sequentially by thermal evaporation under ~10^{-5} Pa, where the photoactive area of the cells was 0.126 cm^2. The *J–V* characteristics of the cells were measured using a Keithley 2400 source–measure unit in nitrogen atmosphere under the 1 sun (AM1.5G) condition using a solar simulator (SAN-EI Electric, XES-40S1). Light intensity was calibrated with a reference PV cell (KONICA MINOLTA AK-100 certified by National Institute of Advanced Industrial Science and Technology, Japan). EQE spectra were measured with a spectral response measuring system (SOMA OPTICS, S-9241). More than 10 different substrates (four photoactive areas each) were prepared, and their photovoltaic properties were measured. Photoactive layer thickness was measured with an ET4000 (Kosaka Laboratory, Ltd.).

ASSOCIATED CONTENT

Supporting Information

The Supporting Information is available free of charge on the ACS Publications website at DOI:XXX. Measurements, cyclic voltammograms, solar cell properties, 2D GIXD patterns, absorption spectra, optical constants, simulated reflection absorption spectra, properties for hole- and electron-only devices, transient absorption spectra, solar cell stability test

AUTHOR INFORMATION

Corresponding authors

*d_yokoyama@yz.yamagata-u.ac.jp

*ohkita@photo.polym.kyoto-u.ac.jp

*iosaka@hiroshima-u.ac.jp

Notes

The authors declare no competing financial interest.

ACKNOWLEGEMENTS

This research was supported by Advanced Low Carbon Technology Research and Development Program (ALCA) of Japan Science and Technology Agency (Grant No. JPMJAL 1404), “Next Generation Photovoltaics” Promising Research Initiatives in Hiroshima University (the Program for Enhancement of Research Universities from the Ministry of Education, Culture, Sports, Science, and Technology (MEXT)), Grant-in-Aid for Scientific Research from Japan Society for the Promotion of Science (No. 19K21129), and Futaba Research Grant Program. 2D GIXD experiments were performed at SPring-8 with the approval of the Japan Synchrotron Radiation Research Institute (Proposal Nos. 2017A1771, 2017B1831, and 2018A1747). We thank Dr Y. Wang for part of the PYS measurements. We are grateful to Dr T. Koganezawa for support in the GIXD measurement.

REFERENCES

1. Brabec, C.; Scherf, U.; Dyakonov, N., Organic Photovoltaics. **2014**, I-XVIII.
2. Günes, S.; Neugebauer, H.; Sariciftci, N. S., Conjugated Polymer-Based Organic Solar Cells. *Chem. Rev.* **2007,** *107* (4), 1324-1338.
3. Winder, C.; Sariciftci, N. S., Low bandgap polymers for photon harvesting in bulk heterojunction solar cells. *J. Mater. Chem.* **2004,** *14* (7), 1077-1086.
4. Mühlbacher, D.; Scharber, M.; Morana, M.; Zhu, Z.; Waller, D.; Gaudiana, R.; Brabec, C., High Photovoltaic Performance of a Low-Bandgap Polymer. *Adv. Mater.* **2006,** *18* (21), 2884-2889.
5. Zhou, E.; Wei, Q.; Yamakawa, S.; Zhang, Y.; Tajima, K.; Yang, C.; Hashimoto, K., Diketopyrrolopyrrole-Based Semiconducting Polymer for Photovoltaic Device with Photocurrent Response Wavelengths up to 1.1 μm. *Macromolecules* **2010,** *43* (2), 821-826.
6. Liang, Y.; Xu, Z.; Xia, J.; Tsai, S.-T.; Wu, Y.; Li, G.; Ray, C.; Yu, L., For the Bright Future—Bulk Heterojunction Polymer Solar Cells with Power Conversion Efficiency of 7.4%. *Adv. Mater.* **2010,** *22* (20), E135-E138.
7. Osaka, I.; Shimawaki, M.; Mori, H.; Doi, I.; Miyazaki, E.; Koganezawa, T.; Takimiya, K., Synthesis, Characterization, and Transistor and Solar Cell Applications of a Naphthobisthiadiazole-Based Semiconducting Polymer. *J. Am. Chem. Soc.* **2012,** *134* (7), 3498-3507.
8. Dou, L.; Liu, Y.; Hong, Z.; Li, G.; Yang, Y., Low-Bandgap Near-IR Conjugated Polymers/Molecules for Organic Electronics. *Chem. Rev.* **2015,** *115* (23), 12633-12665.
9. Liu, C.; Wang, K.; Gong, X.; Heeger, A. J., Low bandgap semiconducting polymers for polymeric photovoltaics. *Chem. Soc. Rev.* **2016,** *45* (17), 4825-4846.
10. Lee, C.; Lee, S.; Kim, G.-U.; Lee, W.; Kim, B. J., Recent Advances, Design Guidelines, and Prospects of All-Polymer Solar Cells. *Chem. Rev.* **2019,** *119* (13), 8028-8086.
11. Hou, J.; Inganäs, O.; Friend, R. H.; Gao, F., Organic solar cells based on non-fullerene acceptors. *Nat. Mater.* **2018,** *17*, 119.
12. Zhang, J.; Tan, H. S.; Guo, X.; Facchetti, A.; Yan, H., Material insights and challenges for non-fullerene organic solar cells based on small molecular acceptors. *Nat. Energy* **2018,** *3* (9), 720-731.
13. Wadsworth, A.; Moser, M.; Marks, A.; Little, M. S.; Gasparini, N.; Brabec, C. J.; Baran, D.; McCulloch, I., Critical review of the molecular design progress in non-fullerene electron acceptors towards commercially viable organic solar cells. *Chem. Soc. Rev.* **2019,** *48* (6), 1596-1625.
14. Schilinsky, P.; Waldauf, C.; Brabec, C. J., Recombination and loss analysis in polythiophene based bulk heterojunction photodetectors. *Appl. Phys. Lett.* **2002,** *81* (20), 3885-3887.
15. Li, G.; Shrotriya, V.; Huang, J.; Yao, Y.; Moriarty, T.; Emery, K.; Yang, Y., High-efficiency solution processable polymer photovoltaic cells by self-organization of polymer blends. *Nat. Mater.* **2005,** *4* (11), 864-868.
16. White, M. S.; Olson, D. C.; Shaheen, S. E.; Kopidakis, N.; Ginley, D. S., Inverted bulk-heterojunction organic photovoltaic device using a solution-derived ZnO underlayer. *Appl. Phys. Lett.*

2006, *89* (14), 143517.

17. Peet, J.; Wen, L.; Byrne, P.; Rodman, S.; Forberich, K.; Shao, Y.; Drolet, N.; Gaudiana, R.; Dennler, G.; Waller, D., Bulk heterojunction solar cells with thick active layers and high fill factors enabled by a bithiophene-co-thiazolothiazole push-pull copolymer. *Appl. Phys. Lett.* **2011,** *98* (4), 043301.

18. Price, S. C.; Stuart, A. C.; Yang, L.; Zhou, H.; You, W., Fluorine Substituted Conjugated Polymer of Medium Band Gap Yields 7% Efficiency in Polymer−Fullerene Solar Cells. *J. Am. Chem. Soc.* **2011,** *133* (12), 4625-4631.

19. Li, W.; Hendriks, K. H.; Roelofs, W. S. C.; Kim, Y.; Wienk, M. M.; Janssen, R. A. J., Efficient Small Bandgap Polymer Solar Cells with High Fill Factors for 300 nm Thick Films. *Adv. Mater.* **2013,** *25* (23), 3182-3186.

20. Osaka, I.; Kakara, T.; Takemura, N.; Koganezawa, T.; Takimiya, K., Naphthodithiophene–Naphthobisthiadiazole Copolymers for Solar Cells: Alkylation Drives the Polymer Backbone Flat and Promotes Efficiency. *J. Am. Chem. Soc.* **2013,** *135* (24), 8834-8837.

21. Osaka, I.; Saito, M.; Koganezawa, T.; Takimiya, K., Thiophene–Thiazolothiazole Copolymers: Significant Impact of Side Chain Composition on Backbone Orientation and Solar Cell Performances. *Adv. Mater.* **2014,** *26* (2), 331-338.

22. Vohra, V.; Kawashima, K.; Kakara, T.; Koganezawa, T.; Osaka, I.; Takimiya, K.; Murata, H., Efficient inverted polymer solar cells employing favourable molecular orientation. *Nat. Photonics* **2015,** *9*, 403.

23. Saito, M.; Koganezawa, T.; Osaka, I., Correlation between Distribution of Polymer Orientation and Cell Structure in Organic Photovoltaics. *ACS Appl. Mater. Interfaces* **2018,** *10* (38), 32420-32425.

24. He, Z.; Zhong, C.; Su, S.; Xu, M.; Wu, H.; Cao, Y., Enhanced power-conversion efficiency in polymer solar cells using an inverted device structure. *Nat. Photonics* **2012,** *6*, 591.

25. He, Z.; Xiao, B.; Liu, F.; Wu, H.; Yang, Y.; Xiao, S.; Wang, C.; Russell, T. P.; Cao, Y., Single-junction polymer solar cells with high efficiency and photovoltage. *Nat. Photonics* **2015,** *9* (3), 174-179.

26. Sievers, D. W.; Shrotriya, V.; Yang, Y., Modeling optical effects and thickness dependent current in polymer bulk-heterojunction solar cells. *J. Appl. Phys.* **2006,** *100* (11), 114509.

27. Burkhard, G. F.; Hoke, E. T.; McGehee, M. D., Accounting for Interference, Scattering, and Electrode Absorption to Make Accurate Internal Quantum Efficiency Measurements in Organic and Other Thin Solar Cells. *Adv. Mater.* **2010,** *22* (30), 3293-3297.

28. Armin, A.; Yazmaciyan, A.; Hambsch, M.; Li, J.; Burn, P. L.; Meredith, P., Electro-Optics of Conventional and Inverted Thick Junction Organic Solar Cells. *ACS Photonics* **2015,** *2* (12), 1745-1754.

29. Ameri, T.; Khoram, P.; Min, J.; Brabec, C. J., Organic Ternary Solar Cells: A Review. *Adv. Mater.* **2013,** *25* (31), 4245-4266.

30. Cheng, P.; Zhan, X., Versatile third components for efficient and stable organic solar cells. *Mater. Horiz.* **2015,** *2* (5), 462-485.

31. Lu, L.; Kelly, M. A.; You, W.; Yu, L., Status and prospects for ternary organic photovoltaics. *Nat. Photonics* **2015,** *9* (8), 491-500.

32. An, Q.; Zhang, F.; Zhang, J.; Tang, W.; Deng, Z.; Hu, B., Versatile ternary organic solar cells: a critical review. *Energy Environ. Sci.* **2016,** *9* (2), 281-322.

33. Huang, W.; Cheng, P.; Yang, Y.; Li, G.; Yang, Y., High-Performance Organic Bulk-Heterojunction Solar Cells Based on Multiple-Donor or Multiple-Acceptor Components. *Adv. Mater.* **2018,** *30* (8), 1705706.

34. Gasparini, N.; Salleo, A.; McCulloch, I.; Baran, D., The role of the third component in ternary organic solar cells. *Nature Reviews Materials* **2019,** *4* (4), 229-242.

35. Lee, J.; Lee, S. M.; Chen, S.; Kumari, T.; Kang, S.-H.; Cho, Y.; Yang, C., Organic Photovoltaics with Multiple Donor–Acceptor Pairs. *Adv. Mater.* **2019,** *31* (20), 1804762.

36. Peet, J.; Tamayo, A. B.; Dang, X. D.; Seo, J. H.; Nguyen, T. Q., Small molecule sensitizers for near-infrared absorption in polymer bulk heterojunction solar cells. *Appl. Phys. Lett.* **2008,** *93* (16), 163306.

37. Wang, Y.; Wang, T.; Chen, J.; Kim, H. D.; Gao, P.; Wang, B.; Iriguchi, R.; Ohkita, H., Quadrupolar D–A–D diketopyrrolopyrrole-based small molecule for ternary blend polymer solar cells. *Dyes Pigm.* **2018,** *158*, 213-218.

38. Honda, S.; Nogami, T.; Ohkita, H.; Benten, H.; Ito, S., Improvement of the Light-Harvesting Efficiency in Polymer/Fullerene Bulk Heterojunction Solar Cells by Interfacial Dye Modification. *ACS Appl. Mater. Interfaces* **2009,** *1* (4), 804-810.

39. Honda, S.; Ohkita, H.; Benten, H.; Ito, S., Multi-colored dye sensitization of polymer/fullerene bulk heterojunction solar cells. *Chem. Commun.* **2010,** *46* (35), 6596-6598.

40. Honda, S.; Yokoya, S.; Ohkita, H.; Benten, H.; Ito, S., Light-Harvesting Mechanism in Polymer/Fullerene/Dye Ternary Blends Studied by Transient Absorption Spectroscopy. *J. Phys. Chem. C* **2011,** *115* (22), 11306-11317.

41. Honda, S.; Ohkita, H.; Benten, H.; Ito, S., Selective Dye Loading at the Heterojunction in Polymer/Fullerene Solar Cells. *Adv. Energy Mater.* **2011,** *1* (4), 588-598.

42. Xu, H.; Ohkita, H.; Tamai, Y.; Benten, H.; Ito, S., Interface Engineering for Ternary Blend Polymer Solar Cells with a Heterostructured Near-IR Dye. *Adv. Mater.* **2015,** *27* (39), 5868-5874.

43. Huang, J.-S.; Goh, T.; Li, X.; Sfeir, M. Y.; Bielinski, E. A.; Tomasulo, S.; Lee, M. L.; Hazari, N.; Taylor, A. D., Polymer bulk heterojunction solar cells employing Förster resonance energy transfer. *Nat. Photonics* **2013,** *7* (6), 479-485.

44. Zhu, L.; Wang, R.; Qiao, J.; Wu, F., Enhanced photovoltaic performance of ternary solar cells by doping a new squaraine derivative. *Dyes Pigm.* **2016,** *132*, 20-26.

45. Lim, B.; Bloking, J. T.; Ponec, A.; McGehee, M. D.; Sellinger, A., Ternary Bulk Heterojunction Solar Cells: Addition of Soluble NIR Dyes for Photocurrent Generation beyond 800

nm. *ACS Appl. Mater. Interfaces* **2014,** *6* (9), 6905-6913.

46. Savoie, B. M.; Dunaisky, S.; Marks, T. J.; Ratner, M. A., The Scope and Limitations of Ternary Blend Organic Photovoltaics. *Adv. Energy Mater.* **2015,** *5* (3), 1400891.

47. Saito, M.; Koganezawa, T.; Osaka, I., Understanding Comparable Charge Transport Between Edge-on and Face-on Polymers in a Thiazolothiazole Polymer System. *ACS Appl. Poly. Mater.* **2019,** *1* (6), 1257-1262.

48. Lin, Y.; Wang, J.; Zhang, Z.-G.; Bai, H.; Li, Y.; Zhu, D.; Zhan, X., An Electron Acceptor Challenging Fullerenes for Efficient Polymer Solar Cells. *Adv. Mater.* **2015,** *27* (7), 1170-1174.

49. Zhao, W.; Li, S.; Yao, H.; Zhang, S.; Zhang, Y.; Yang, B.; Hou, J., Molecular Optimization Enables over 13% Efficiency in Organic Solar Cells. *J. Am. Chem. Soc.* **2017,** *139* (21), 7148-7151.

50. Li, S.; Ye, L.; Zhao, W.; Zhang, S.; Mukherjee, S.; Ade, H.; Hou, J., Energy-Level Modulation of Small-Molecule Electron Acceptors to Achieve over 12% Efficiency in Polymer Solar Cells. *Adv. Mater.* **2016,** *28* (42), 9423-9429.

51. Yao, H.; Cui, Y.; Yu, R.; Gao, B.; Zhang, H.; Hou, J., Design, Synthesis, and Photovoltaic Characterization of a Small Molecular Acceptor with an Ultra-Narrow Band Gap. *Angew. Chem. Int. Ed.* **2017,** *56* (11), 3045-3049.

52. Yoshida, H., Near-ultraviolet inverse photoemission spectroscopy using ultra-low energy electrons. *Chem. Phys. Lett.* **2012,** *539-540*, 180-185.

53. Yoshida, H., Principle and application of low energy inverse photoemission spectroscopy: A new method for measuring unoccupied states of organic semiconductors. *J. Electron Spectrosc. Relat. Phenom.* **2015,** *204*, 116-124.

54. Veldman, D.; Meskers, S. C. J.; Janssen, R. A. J., The Energy of Charge-Transfer States in Electron Donor–Acceptor Blends: Insight into the Energy Losses in Organic Solar Cells. *Adv. Funct. Mater.* **2009,** *19* (12), 1939-1948.

55. King, R. R.; Bhusari, D.; Boca, A.; Larrabee, D.; Liu, X. Q.; Hong, W.; Fetzer, C. M.; Law, D. C.; Karam, N. H., Band gap-voltage offset and energy production in next-generation multijunction solar cells. *Prog Photovolt Res Appl.* **2011,** *19* (7), 797-812.

56. Wang, M.; Wang, H.; Yokoyama, T.; Liu, X.; Huang, Y.; Zhang, Y.; Nguyen, T.-Q.; Aramaki, S.; Bazan, G. C., High Open Circuit Voltage in Regioregular Narrow Band Gap Polymer Solar Cells. *J. Am. Chem. Soc.* **2014,** *136* (36), 12576-12579.

57. Han, G.; Yi, Y., Origin of Photocurrent and Voltage Losses in Organic Solar Cells. *Adv. Theory Simul.* **2019,** *2* (8), 1900067.

58. Kawashima, K.; Tamai, Y.; Ohkita, H.; Osaka, I.; Takimiya, K., High-efficiency polymer solar cells with small photon energy loss. *Nature Commun.* **2015,** *6*, 10085.

59. Li, W.; Hendriks, K. H.; Furlan, A.; Wienk, M. M.; Janssen, R. A. J., High Quantum Efficiencies in Polymer Solar Cells at Energy Losses below 0.6 eV. *J. Am. Chem. Soc.* **2015,** *137* (6), 2231-2234.

60. Liu, J.; Chen, S.; Qian, D.; Gautam, B.; Yang, G.; Zhao, J.; Bergqvist, J.; Zhang, F.; Ma, W.;

Ade, H.; Inganäs, O.; Gundogdu, K.; Gao, F.; Yan, H., Fast charge separation in a non-fullerene organic solar cell with a small driving force. *Nat. Energy* **2016,** *1*, 16089.

61. Yao, Z.; Liao, X.; Gao, K.; Lin, F.; Xu, X.; Shi, X.; Zuo, L.; Liu, F.; Chen, Y.; Jen, A. K. Y., Dithienopicenocarbazole-Based Acceptors for Efficient Organic Solar Cells with Optoelectronic Response Over 1000 nm and an Extremely Low Energy Loss. *J. Am. Chem. Soc.* **2018,** *140* (6), 2054-2057.

62. Yokoyama, D.; Qiang Wang, Z.; Pu, Y.-J.; Kobayashi, K.; Kido, J.; Hong, Z., High-efficiency simple planar heterojunction organic thin-film photovoltaics with horizontally oriented amorphous donors. *Sol. Energy Mater. Sol. Cells* **2012,** *98*, 472-475.

63. Ohkita, H.; Ito, S., Transient absorption spectroscopy of polymer-based thin-film solar cells. *Polymer* **2011,** *52* (20), 4397-4417.

64. Roe, R.-J., Methods of X-Ray and Neutron Scattering in Polymer Science. *Oxford University Press* **2010**.

65. Reese, M. O.; Gevorgyan, S. A.; Jørgensen, M.; Bundgaard, E.; Kurtz, S. R.; Ginley, D. S.; Olson, D. C.; Lloyd, M. T.; Morvillo, P.; Katz, E. A.; Elschner, A.; Haillant, O.; Currier, T. R.; Shrotriya, V.; Hermenau, M.; Riede, M.; R. Kirov, K.; Trimmel, G.; Rath, T.; Inganäs, O.; Zhang, F.; Andersson, M.; Tvingstedt, K.; Lira-Cantu, M.; Laird, D.; McGuiness, C.; Gowrisanker, S.; Pannone, M.; Xiao, M.; Hauch, J.; Steim, R.; DeLongchamp, D. M.; Rösch, R.; Hoppe, H.; Espinosa, N.; Urbina, A.; Yaman-Uzunoglu, G.; Bonekamp, J.-B.; van Breemen, A. J. J. M.; Girotto, C.; Voroshazi, E.; Krebs, F. C., Consensus stability testing protocols for organic photovoltaic materials and devices. *Sol. Energy Mater. Sol. Cells* **2011,** *95* (5), 1253-1267.

66. Saito, M.; Osaka, I.; Suzuki, Y.; Takimiya, K.; Okabe, T.; Ikeda, S.; Asano, T., Highly Efficient and Stable Solar Cells Based on Thiazolothiazole and Naphthobisthiadiazole Copolymers. *Sci. Rep.* **2015,** *5*, 14202.

67. Saito, M.; Osaka, I., Impact of side chain placement on thermal stability of solar cells in thiophene–thiazolothiazole polymers. *J. Mater. Chem. C* **2018,** *6* (14), 3668-3674.

68. Osaka, I.; Saito, M.; Mori, H.; Koganezawa, T.; Takimiya, K., Drastic change of molecular orientation in a thiazolothiazole copolymer by molecular-weight control and blending with $PC_{61}BM$ leads to high efficiencies in solar cells. *Adv Mater* **2012,** *24* (3), 425-430.